Electronic Supplementary Information (ESI): for

Ultra-low thermal conductivity and enhanced mechanical properties of High-Entropy Perovskite Ceramics

Wenjing Qiao[1], Jiantuo Zhao[1], Yingwei Qi[2], Xiaopei Zhu[3], Xifei Wang[1], Zhizhi Xu[1], Mei Bai[1], Junwen Mei[1], Yanhua Hu[2]* and Xiaojie Lou[1]*

[1] State Key Laboratory for Mechanical Behavior of Materials, and Frontier Institute of Science and Technology, Xi'an Jiaotong University, Xi'an 710049, China

[2] Department of Chemical Engineering, Ordos Institute of Technology, Ordos 017000, P. R. China

[3] School of Materials Science and Engineering, Xi 'an University of Technology

**Corresponding author's email address: aoqibaby080410@163.com (Y.H. Hu); xlou03@mail.xjtu.edu.cn (X.J. Lou)*

Table S1 The coordination number (C.N.) of each element, the corresponding ionic radius and valence state.

Site	Element	C.N.	ionic radius /[Å]	valence state
A-site	Ba	12	1.61	2+
B-site	Zr	6	0.72	4+
	Ti	6	0.605	4+
	Sn	6	0.69	4+
	Hf	6	0.71	4+
	Nb	6	0.68	4+
	O	6	1.40	2-

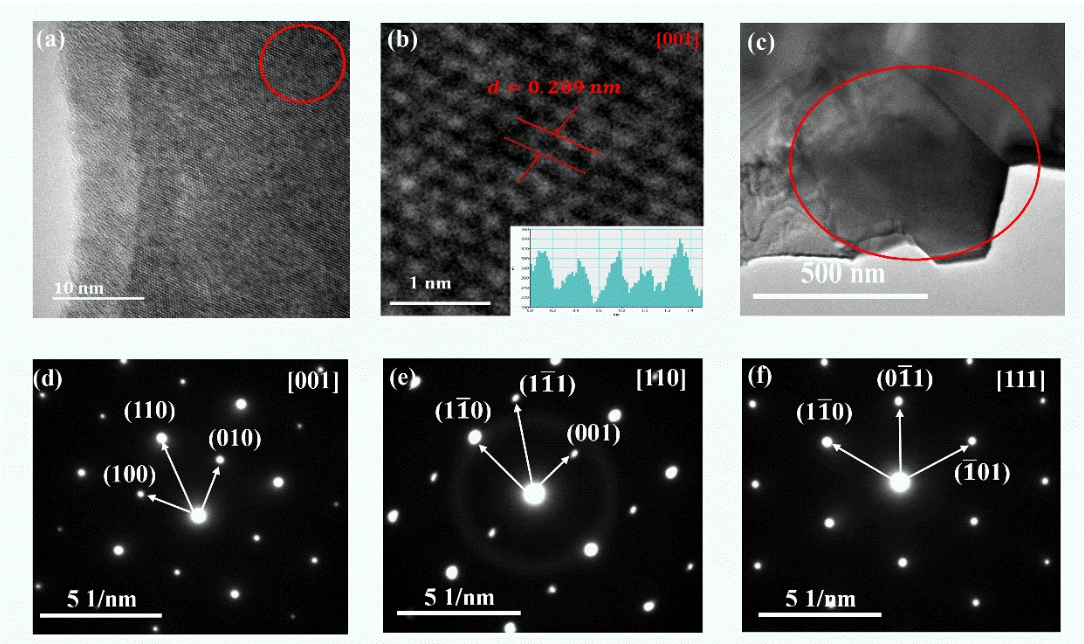

Fig. S1. TEM analysis of HEC-Nb ceramic. (a) HRTEM image and (b) the corresponding enlarged image, (c) Bright-field TEM image and (d-f) SAED patterns of lattice fringes with different directions.

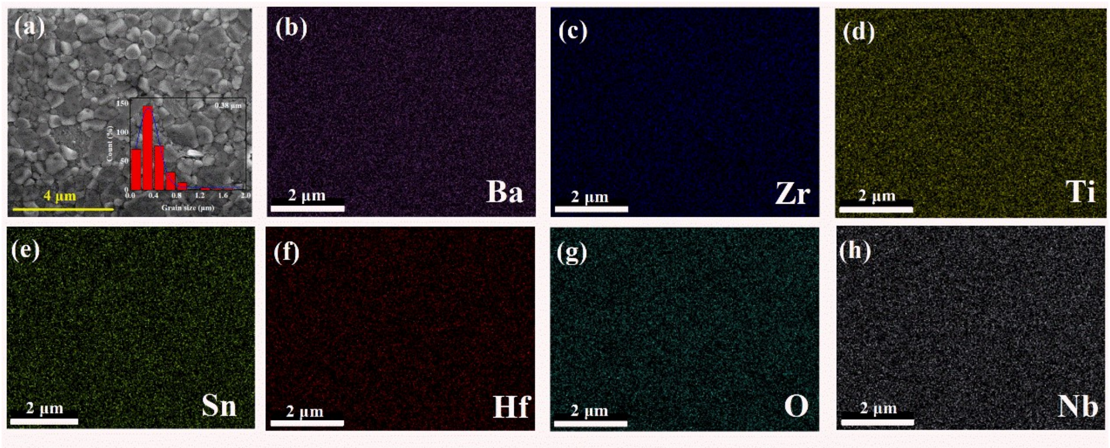

Fig. S2. (a) SEM images, and (b-h) EDS mapping of the HEC-Nb high-entropy ceramics.

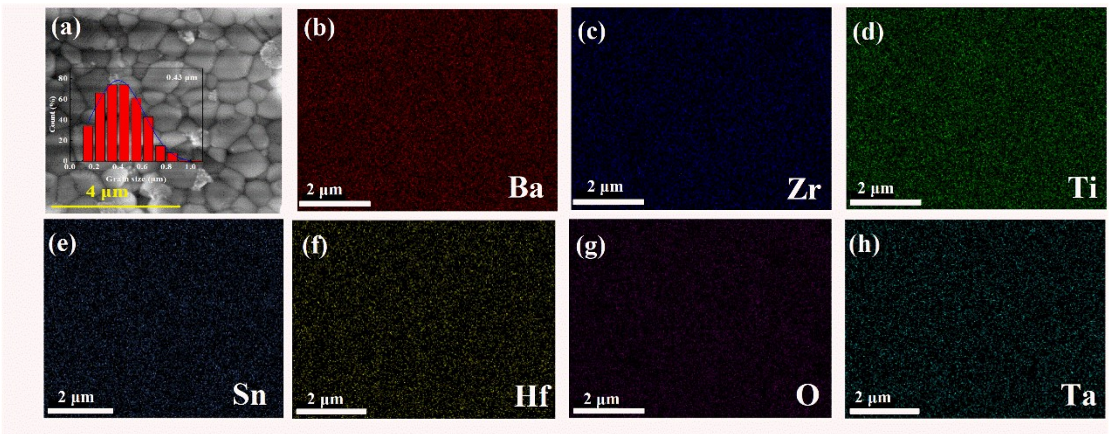

Fig. S3. (a) SEM images, and (b-h) EDS mapping of the HEC-Ta high-entropy ceramics.

The homogeneous distribution of the five elements in the grains is indicative of the absence of element segregation, as evidenced by the EDS mappings. This finding confirms the formation of a solid solution, with a single solid solution phase being present in the sintered compact.

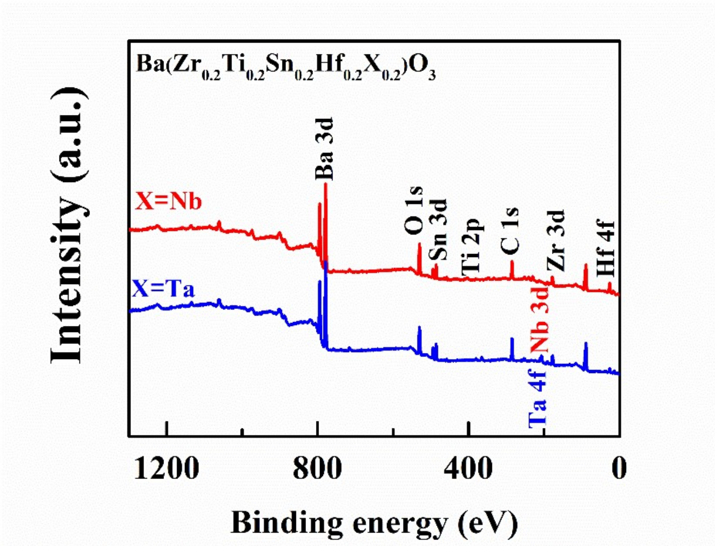

Fig. S4. XPS survey spectra of $Ba(Zr_{0.2}Ti_{0.2}Sn_{0.2}Hf_{0.2}X_{0.2})O_3$ (X= Nb, Ta).

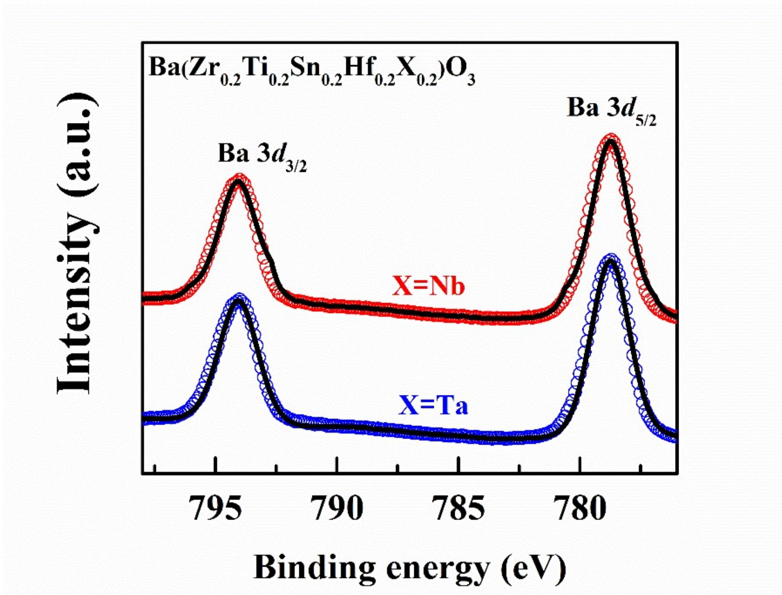

Fig. S5. XPS survey spectra of Ba 3*d*.

Two primary peaks corresponding to Ba $3d_{5/2}$ and Ba $3d_{3/2}$ were observed for $Ba(Zr_{0.2}Ti_{0.2}Sn_{0.2}Hf_{0.2}X_{0.2})O_3$ (X = Nb^{+},Ta^{+}) ceramics due to the spin-orbit coupling effect [1].

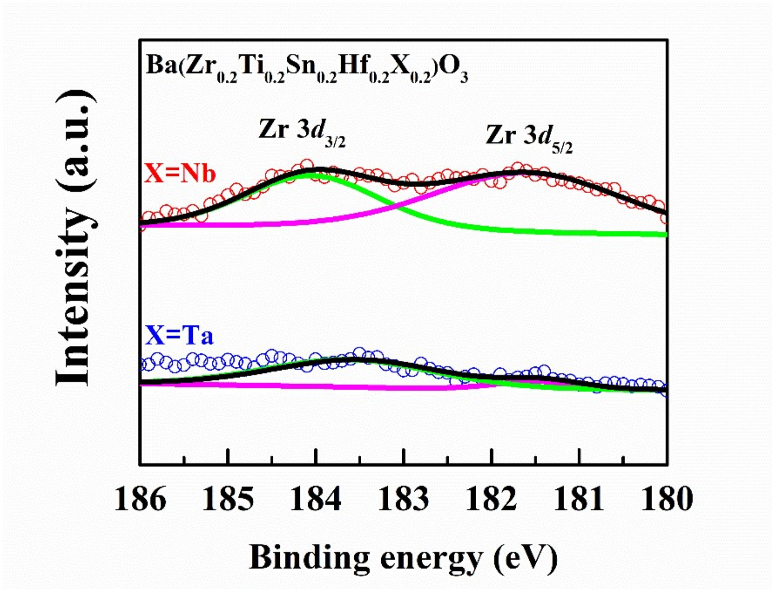

Fig. S6. XPS survey spectra of Zr 3*d*.

Apart from the peaks from Ba 4$p_{3/2}$, two primary peaks for Zr 3*d* (Zr 3$d_{5/2}$ and Zr 3$d_{3/2}$) were observed for $Ba(Zr_{0.2}Ti_{0.2}Sn_{0.2}Hf_{0.2}X_{0.2})O_3$ (X = Nb^+,Ta^+) ceramics due to the spin-orbit coupling effect [2].

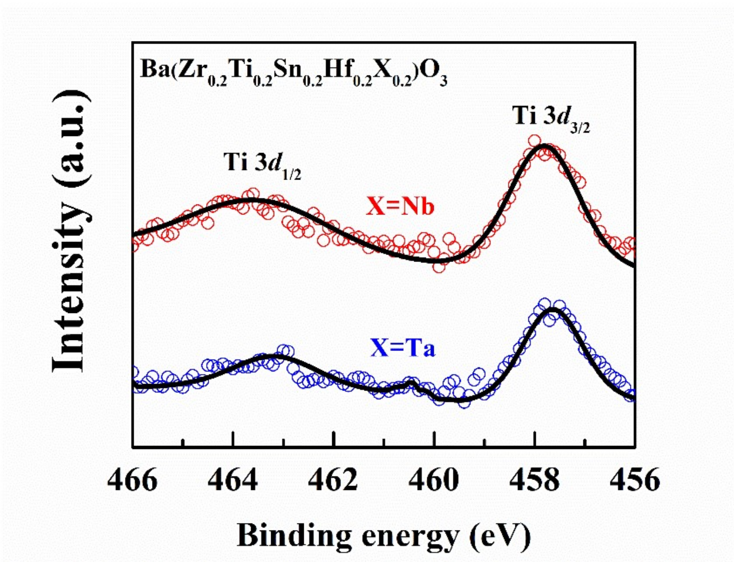

Fig. S7. XPS survey spectra of Ti 3*d*.

Two primary peaks namely Ti 2$p_{3/2}$ and Ti 2$p_{1/2}$ were observed for $Ba(Zr_{0.2}Ti_{0.2}Sn_{0.2}Hf_{0.2}X_{0.2})O_3$ (X = Nb^+,Ta^+) ceramics due to the spin-orbit coupling effect [3].

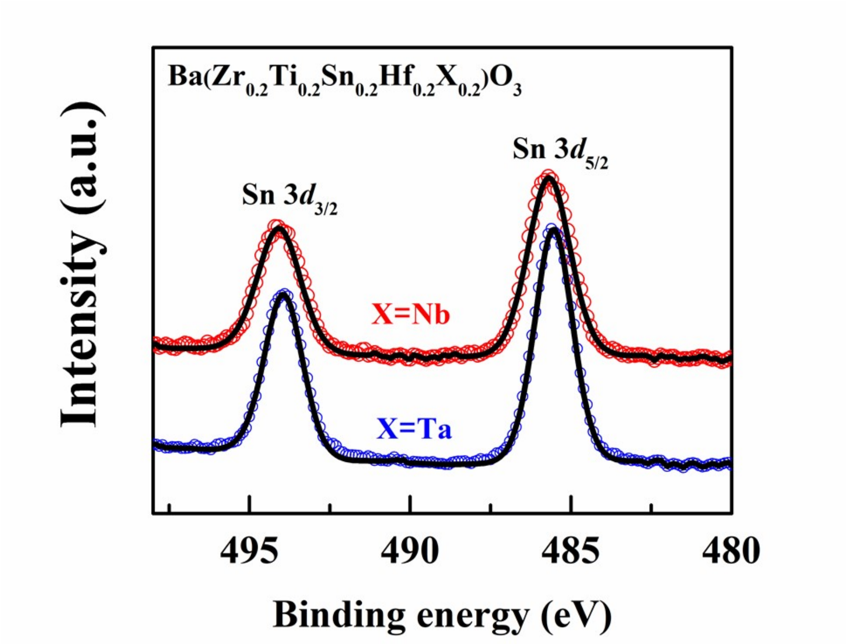

Fig. S8. XPS survey spectra of Sn 3*d*.

Two primary peaks namely Sn 3$d_{5/2}$ and Sn 3$d_{3/2}$ were observed for $Ba(Zr_{0.2}Ti_{0.2}Sn_{0.2}Hf_{0.2}X_{0.2})O_3$ (X = Nb^+,Ta^+) ceramics due to the spin-orbit coupling effect [4].

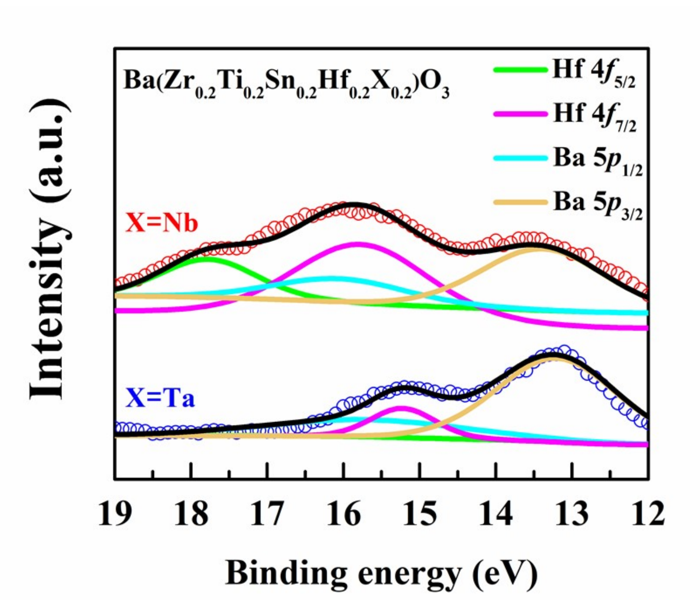

Fig. S9. XPS survey spectra of *Hf 4f.*

Due to the overlapping signals of Ba 5*p* and Hf 4*f*, it was necessary to deconvolute the curves into four peaks. In addition to the peaks originating from Ba 5*p*, two additional peaks were observed from Hf 4$f_{7/2}$ and Hf 3$d_{5/2}$, respectively[1].

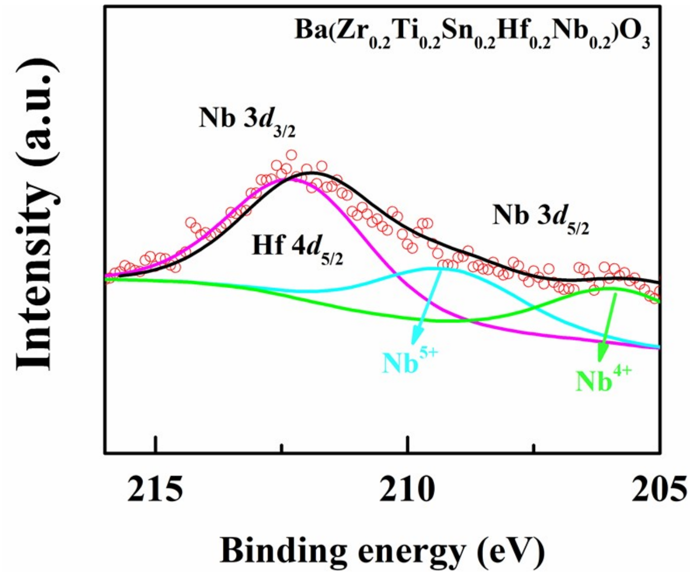

Fig. S10. XPS survey spectra of Nb 3*d*.

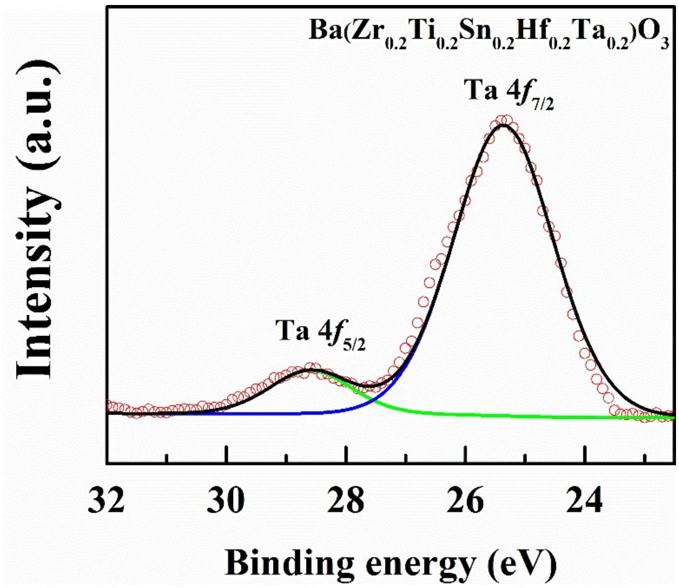

Fig. S11. XPS survey spectra of Ta 4*f*.

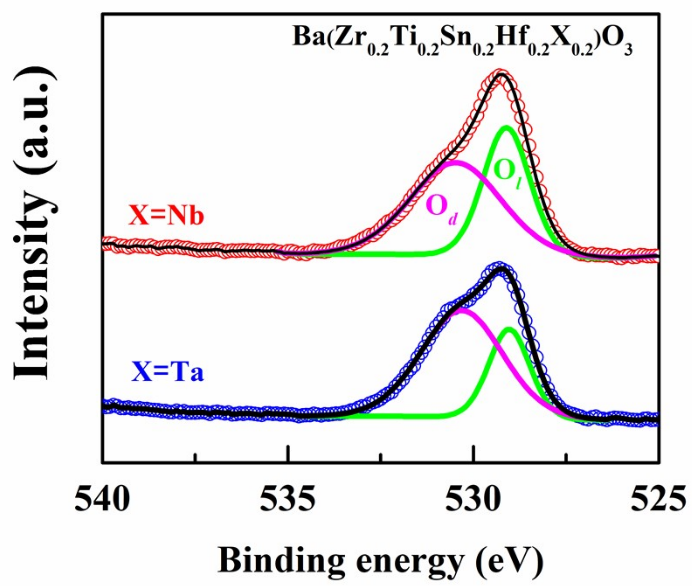

Fig. S12. XPS survey spectra of O 2*p.*

References:

1. J. Wang and B. Luo, *Physica B: Condensed Matter*, 2021, **601**, 412586.
2. H. Ikawa, T. Yamada, K. Kojima and S. Matsumoto, *Journal of the American Ceramic Society*, 1991, **74**, 1459-1462.
3. M. C. Biesinger, B. P. Payne, A. P. Grosvenor, L. W. Lau, A. R. Gerson and R. S. C. Smart, *Applied Surface Science*, 2011, **257**, 2717-2730.
4. O. Renault, D. Samour, D. Rouchon, P. Holliger, A.-M. Papon, D. Blin and S. Marthon, *Thin Solid Films*, 2003, **428**, 190-194.